

DESY SR 84-28

November 1984

CONTRAST INVESTIGATIONS OF SURFACE ACOUSTIC WAVES BY
STROBOSCOPIC TOPOGRAPHY II. WAVEFIELD DEVIATION CONTRAST

by

H. Cerva, W. Graeff

Hamburger Synchrotronstrahlungslabor HASYLAB at DESY, Hamburg

| | | |
|-----------------------------|---------------|-----------------------|
| Eigentum der Property of | DESY | Bibliothek library |
| Zugang: Accessions: | 28. NOV. 1984 | |
| Leihfrist: Loan period: | 7 | Tage days |

ISSN 0723-7979

DESY behält sich alle Rechte für den Fall der Schutzrechtserteilung und für die wirtschaftliche Verwertung der in diesem Bericht enthaltenen Informationen vor.

DESY reserves all rights for commercial use of information included in this report, especially in case of filing application for or grant of patents.

To be sure that your preprints are promptly included in the
HIGH ENERGY PHYSICS INDEX ,
send them to the following address (if possible by air mail) :

DESY
Bibliothek
Notkestrasse 85
2 Hamburg 52
Germany

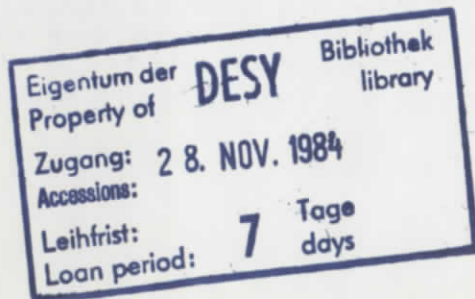
CONTRAST INVESTIGATIONS OF SURFACE ACOUSTIC WAVES BY STROBOSCOPIC
TOPOGRAPHY II. WAVEFIELD DEVIATION CONTRAST

H. Cerva (a)
W. Graeff

Hamburger Synchrotronstrahlungslabor HASYLAB
at
Deutsches Elektronensynchrotron DESY
2000 Hamburg 52, Germany.

(a) on leave from
Institut für Angewandte und Technische Physik
Technische Universität Wien
1040 Wien, Austria.

submitted to: phys. stat. sol.



ABSTRACT

When imaging a surface acoustic wave by stroboscopic X-ray topography a contrast contribution exists which can be related to the deviation of X-ray beams in the deformation field of the acoustic wave. With narrow entrance slits this contribution can be separated from the surface reflected waves. Using a beam path theory of Bonse the beam trajectories inside the crystal and the intensity profiles at the surface are calculated. It is also demonstrated that this contrast which has two nearly equal peaks within the acoustic period turns to the orientation contrast with one peak per period when increasing the distance between sample and film.

Bei der Abbildung von akustischen Oberflächenwellen mit stroboskopischer Röntgentopographie tritt ein Kontrastbeitrag auf, der auf die Umlenkung von Röntgenstrahlen im Deformationsfeld der akustischen Welle zurückzuführen ist. Mit Hilfe von engen Eintrittsspalten läßt sich dieser Anteil getrennt vom oberflächenreflektierten Strahl darstellen. Mit einer Strahlwegtheorie nach Bonse lassen sich Strahlverläufe im Kristallinnern und Intensitätsverteilungen an der Oberfläche berechnen. Es wird ebenfalls gezeigt, daß dieser Kontrast, der innerhalb einer akustischen Periode zwei annähernd gleich hohe Maxima hat, mit wachsendem Abstand zwischen Probe und Film in den Orientierungskontrast mit nur einem Maximum pro Periode übergeht.

Classification:

7.; 14.4.1; 22.8.1

1. INTRODUCTION

In Part I of this paper [1] the authors explained the mechanism how travelling surface acoustic waves (SAW) propagating on a YZ-LiNbO₃ crystal can be visualized by stroboscopic synchrotron X-ray topography. The corrugated surface formed by the SAW reflects the X-rays such that wave troughs bring the X-rays into focus whereas the wave crests defocalize. This orientation contrast results in a periodic intensity pattern on the topograph with the periodicity being the SAW wavelength Λ . The experiments described in Part I indicated an additional contribution to the SAW contrast due to the deviation of X-ray wavefields by the acoustic strain field inside the crystal so that they can emerge again at the entrance surface.

It is the aim of this paper to give further experimental evidence of this special contrast and treat this phenomenon with a dynamical X-ray diffraction theory developed for slightly distorted crystals [2]. Numerical calculations will give trajectories of wavefield beams in the SAW strain field and the correspondence with the experiments will be discussed.

2. EXPERIMENTS.

The experimental setup used to image SAW and the formation of orientation contrast were described in detail in Part I. In this section we will set forth what is meant by wavefield deviation and how it can be observed. All topographs have been taken in Bragg case geometry using the (0k0) netplanes as reflecting planes. Whereas the observation of orientation contrast because of its pure geometrical origin is wavelength independent we have chosen for most of the experiments described below the wavelength in such a way that the contribution of the (060) reflection to the deviated intensity was optimized. This was achieved by shifting the wavelength of the (090) reflection slightly below the Nb K-absorption edge at $\lambda = 0.065$ nm so that (030) and (090) contributions were strongly suppressed by absorption.

In our previous paper we indicated that the topograph image of a shadow caused by an object placed in the incident beam is not entirely free from

X-ray intensity when the topographed region is strained by a SAW. So intensity is detected from an area not having been illuminated originally.

A more convincing experiment can be done by collimating the incident beam by a slit of about 10 μm width. The diffraction geometry is chosen such that the SAW propagation vector K and the slit blades are perpendicular to the diffraction plane. The situation is shown in Figure 1(a) where two topographs have been superposed. At first the whole sample was exposed to the synchrotron beam thereby imaging the travelling waves. A subsequent exposure on the same topograph with the slit intersecting the beam gives the accurate position of the slit relative to the acoustic wave. In Figure 1(b) the slit is imaged alone. We see spots of higher intensity marking wave troughs alternating with areas of less intensity marking wave crests. This part of the image is due to orientation contrast but we also observe intensity spikes on one side normal to the slit image. As this region was not illuminated we assume that wavefields having penetrated into the bulk were deviated by the strain field of the SAW and emerged at the entrance surface. We realize that these wavefields reach the surface at the locations of wave troughs only while in the region of wave crests no enhanced intensity is recorded.

A different intensity distribution of these deviated wavefields is shown in Figure 2. These topographs were obtained by rotating the sample about its surface normal (i.e. the Y-axis) by 90° now having the acoustic wave vector K lying in the diffraction plane. In addition to the slit image we can clearly observe deviated intensity in the region of SAW propagation. The excited SAW has a wavelength of approximately 100 μm . Hence it is possible to illuminate different phases of the acoustic wave with a 10 μm wide X-ray beam by introducing an appropriate time delay into the stroboscopic synchronization. The resulting change in the deviated intensity pattern is shown in Figure 2(a-d).

Intensity deviated by the same mechanism in the strain field of built-in dislocations is also visible outside the SAW beam region [3].

3. THEORY OF WAVEFIELD DEVIATION

In order to explain our observations we apply the theory on the propagation of X-ray wavefield beams in slightly deformed crystals [2]. For the sake of brevity it will be summarized only and we will refer to the original paper [2].

The propagation of X-rays inside a crystal is described by so called wavefields which are determined by their tiepoints on the dispersion sur-

face [4]. In Bragg case geometry due to boundary conditions only one wavefield is excited by an incident monochromatic plane wave. It can be described by the amplitude ratio ξ_0 of reflected and transmitted wave in a unique way. Furthermore the propagation direction j of a wavefield with a given ξ_0 can be evaluated from the direction of energy flow (eq. 15b in [2]).

If the deformation of the crystal lattice is small enough so that a locally defined reciprocal lattice vector $h(\mathbf{r})$ is still meaningful the adaption of the wavefield on its way through the deformed crystal to the new lattice orientation will be continuous and can be calculated by variational principles. The path of a wavefield beam with a given initial state ξ_0 is found in an iterative way advancing in steps of length dl along the local direction j . The decrease of beam intensity occurring along each increment dl is evaluated from the absorption coefficient σ_j for propagation in the direction j . Using the local orthonormal axis system f, n, ϵ with n being normal to the Bragg planes and f parallel to them and in the diffraction plane, it turns out that the differential change $d\xi/dl$ is a function of ξ_0 and the factors FF, NN and FN (eq. 56 in [2]). FF, NN and FN describe the local lattice deformation and are to be calculated from the second derivatives $\nabla\nabla(u \cdot n)$ of $(u \cdot n)$ the component of the local displacement vector u normal to the Bragg planes:

$$\begin{aligned} FF &= f \cdot (f \cdot \nabla\nabla(u \cdot n)) \\ NN &= n \cdot (n \cdot \nabla\nabla(u \cdot n)) \\ FN &= f \cdot (n \cdot \nabla\nabla(u \cdot n)) \end{aligned}$$

FF is the reciprocal value of the radius of curvature of the Bragg planes while NN expresses the gradient of the distance of the planes and FN the fanning. With the new value $\xi = \xi_0 + d\xi$ a new direction and absorption coefficient is determined and the iteration cycle commences again.

4. DEFORMATION STATE OF THE CRYSTAL CAUSED BY A SAW.

As we pointed out in Part I we used $(0k0)$ reflexions only, $k = 3, 6$, representing Bragg planes parallel to the YZ-LiNbO₃ surface. For the diffraction geometry of Figure 2 the unit vectors defined in the previous section coincide with the coordinate system commonly used in SAW theory:

$$\begin{aligned} x_1 &= f = 1/c [0001] \\ x_2 &= e = 1/3a [2\bar{1}10] \\ x_3 &= n = 1/\sqrt{3}a [01\bar{1}0] \end{aligned}$$

For YZ-LiNbO₃ the elliptical motion of a volume element is totally confined to the plane $x_2 = 0$. The analytical form of the amplitude u_3 (parallel to

x_3) is given in Part I. Doing stroboscopic topography the crystal is illuminated periodically at a certain point of time. Thus we may set $t = 0$ and u_3 takes the form

$$u_3 = \left\{ \sum C^{(n)} \alpha_3^{(n)} \exp(iKb^{(n)}x_3) \right\} \exp(iKx_1) \left| u_3(0) \right|$$

The meaning of the symbols and numerical values can be found in Table 1 of Part I. The vectors were normalized in order to have $u_3(0) = 1$ at the crystal surface. The factor $|u_3(0)|$ is the magnitude value of the SAW amplitude and is related to the wave excitation power [1]. We obtain for the deformations

$$\begin{aligned} FF &= -K^2 \left\{ \sum C^{(n)} \alpha_3^{(n)} \exp(iKb^{(n)}x_3) \right\} \exp(iKx_1) \left| u_3(0) \right| \\ FN &= -K^2 \left\{ \sum b^{(n)} C^{(n)} \alpha_3^{(n)} \exp(iKb^{(n)}x_3) \right\} \exp(iKx_1) \left| u_3(0) \right| \\ NN &= -K^2 \left\{ \sum b^{(n)2} C^{(n)} \alpha_3^{(n)} \exp(iKb^{(n)}x_3) \right\} \exp(iKx_1) \left| u_3(0) \right| \end{aligned}$$

These expressions are periodic with the surface wavelength Λ and decay in the $-x_3$ direction (see Figure 3). For a wavelength $\Lambda = 100 \mu\text{m}$ and a surface amplitude between 1 and 0.1 nm we find a corresponding radius of curvature between 10 and 100 m. The factor FF dominates obviously the deformation state while the contributions of FN and NN are confined to a very thin surface layer.

5. CALCULATED WAVEFIELD TRAJECTORIES AND INTENSITY PATTERNS.

The theory described above was developed for calculating the path of a wavefield beam through a deformed crystal for incident monochromatic plane waves. For the experimental realization of these assumptions a compromise must be taken between the remaining divergence of the incident 'plane' wave and the collimation of the beam by a narrow slit [5]. If the slit is too narrow the beam divergence is increased due to diffraction to such an extent that the whole dispersion surface is excited in a coherent way [6]. As the theory does not yield the phase change of the wavefield after deviation interference effects can not be accounted for.

In case of a white synchrotron radiation beam impinging on the sample through a narrow slit we may consider a wave with a particular wavelength as nearly plane which means that its divergence is small compared to the angular acceptance of the crystal reflection. This stems from the large distance between crystal and source (34 m). Each of these waves will excite a narrow range of the dispersion surface, described by the parameter y which measures the angular deviation from the kinematical Bragg angle [4]. Although these waves all have the same angle of incidence they are described by different values of y because the Bragg angle changes

with wavelength. As the Fourier coefficients of the dielectric susceptibility are practically constant in the narrow wavelength range the case of a white beam can be accounted for by considering a monochromatic beam with large divergence which excites the dispersion surface in a completely incoherent way. For the numerical calculation in case of a (06.0) reflection and a wavelength $\lambda = 0.09$ nm we used the following values for the Fourier coefficients:

$$\begin{aligned}\chi_{r0} &= -9.3 \cdot 10^{-6} \\ \chi_{rh} &= -2.5 \cdot 10^{-6} - 1.1 \cdot 10^{-7} i \\ \chi_{i0} &= -1.7 \cdot 10^{-7} \\ \chi_{ih} &= -1.6 \cdot 10^{-7} - 0.8 \cdot 10^{-9} i\end{aligned}$$

Figure 4 shows two examples of ray trajectories and corresponding intensity distributions. The step width of the iteration algorithm was adjusted by the programme to the change of ξ in order to save CPU time. The SAW vector K is lying in the diffraction plane. In Figure 4 (a) the position of the incident beam on the sample surface is at a wave trough. Owing to the white radiation lots of independent wavefield trajectories are formed inside the crystal. For clarity only those are shown which either reach the surface or come close to it. Those which reach the surface give rise to a certain amount of 'deviated' intensity which is calculated from the boundary condition. In a rigorous treatment new wavefield beams which are generated at the exit point must be followed. But their contribution to the intensity after a possibly second exit can be neglected.

Along the surface the intensity distribution is plotted. The large peak at the entrance point is the surface reflected intensity of those wave components which already fulfill the reflection condition at the surface. Besides the influence of varying absorption inside the crystal the density of wavefield trajectories at the exit place affects the intensity distribution. In other words due to the inhomogeneous strain field the lateral width of a beam represented by a narrow range of y values (quasi-plane wave) is changed. This was taken into account by distributing the intensity which was calculated for a certain y value between the exit points of the two adjacent y values.

In Figure 4(b) the X-rays hit the crystal in a slightly different position. The wavefields are subjected to a different strain field and two peaks of deviated intensity are formed being approximately $70 \mu\text{m}$ apart. It is interesting to note that some wavefields may change their propagation direction several times. These calculated intensity distributions have to be compared with the topographs in Figure 2.

The calculation does not yield the direction of the deviated beams outside the crystal. That these beams are no longer parallel and hence show some orientation contrast similar to the surface reflected waves is demonstrated in an experiment where the slit is slightly tilted with respect to the surface and topographs in different distances from the sample have been taken. They are shown in Figure 5. At a distance of 5 cm (Figure 5(b)) a series of ripples are seen where every second ripple is slightly more intense than the other ones. With increasing distance the more intense ripples become narrower and even more intense whereas the other ones are spread. At 22 cm we are approximately at the focussing distance of the surface reflected X-rays. This is the case for a SAW with the parameters $\Lambda = 100 \mu\text{m}$, $a_s = 0.35$ nm, $\theta = 37.5^\circ$ and $\beta = 0^\circ$. Hence the orientation contrast dominates the intensity distribution at that distance.

What remains to be explained is the slight difference in intensity of the ripples in Figure 5(b) which is not caused by orientation contrast. A simulation of this topograph is shown in Figure 6. This two-dimensional intensity pattern which shows intensity contour lines has been obtained by calculating the intensity distributions for a number of entrance positions along the oblique slit. The angle of inclination has been exaggerated to spread the distribution along the K vector. The two peaks per period Λ with an intensity difference of about 20 percent are clearly visible. They are not running parallel to the acoustic wave front but form a larger angle with the direct slit image what corresponds well with the experimental findings.

The intensity difference is explained by the anomalous absorption phenomenon in Bragg reflection. This has already been discussed for the case of simple constant deformations in [2] and has been verified experimentally in [4]. If we neglect in our case FN and NN for a qualitative discussion we may take the results from [2] which tell that for $FF > 0$ (a wave trough) the anomalously low absorbed wavefields are bent back to the surface whereas with $FF < 0$ (a wave crest) the anomalously high absorbed wavefields will reach the entrance surface.

In Part I and II of this paper we have explained the origin of the SAW contrast by showing that close to the crystal a contrast dominates which has peaks at both wave crests and troughs and which stems from X-rays passing a fairly thick bulk layer whereas far from the crystal orientation contrast is pronounced having a peak at the wave troughs. It was also demonstrated once again that scanning a sample surface in the Bragg case by a fine collimated slit can reveal information on deformed regions which lie deeper below the surface than the extinction length (here $22 \mu\text{m}$) of the reflection in use. Finally it should be noted that the results of the

beampath theory, which has not been used very often in a quantitative way, again are in excellent agreement with the experimental results.

ACKNOWLEDGEMENTS.

We thank R. Veith and his coworkers of the Siemens AG, München, for the crystals and the possibility to use their facilities for preparation. One of us (H.C.) thanks DESY for financial support during his stay at Hamburg. This work was part of the project No. P 4937 of the Austrian Fond zur Förderung der wissenschaftlichen Forschung.

REFERENCES.

1. H. Cerva and W. Graeff, *phys. stat. sol. (a)* 82, 35 (1984).
2. U. Bonse, *Z. Physik* 177, 385 (1964).
3. U. Bonse, *Z. Physik* 177, 543 (1964).
4. Z.G. Pinsker, *Dynamical Scattering of X-rays in Crystals*, Springer 1978
5. U. Bonse, W. Graeff, *Z. Naturforsch.* 28a, 558 (1973).
6. V.V. Aristov, W. Graeff, V.I. Polovinkina and A.A. Snigirev; to be published

FIGURE CAPTIONS

Figure 1. : Stroboscopic topograph of a SAW on LiNbO_3 , (03-0) reflection, $\theta = 45^\circ$, $\lambda = 0.21 \text{ nm}$, acoustic wavelength $\Lambda = 98.5 \mu\text{m}$, 35.4 MHz. (a) Superposition of full SAW image and slit image to illustrate slit position. (b) Enlarged image of the slit ($10 \mu\text{m}$ slit width). The distance between the bright spots is the acoustic wavelength. Note the faint streaks extending from the spots into the unilluminated area of the crystal surface.

Figure 2. : Slit image of a SAW in different phases (same parameters as in Fig.1). Now the slit is parallel to the wavefronts. W is the width of the SAW beam. The time period of the SAW is 28 ns. The phase delay between (a) and (b) corresponds to 6 ns, between (b) and (c) to 8 ns and between (c) and (d) again 6 ns.

Figure 3. : Iso-deformation lines of (03-0) planes in YZ-LiNbO_3 caused by a SAW. The indicated values of the parameters FF, FN and NN are normalized to $u_3(0) = 1$, the SAW amplitude component at the surface.

Figure 4. : Calculated beampaths and intensity distributions for two different entrance points. For clarity only those beampaths which contribute to the intensity outside and a few typical others are shown.

Figure 5. : Change of the deviated intensity distribution due to orientation contrast. The parameters different from Fig. 1 now have the values: (0k0) reflection, $\theta = 37.5^\circ$, $\lambda = 0.54/k$ nm, $k = 3, 6, 9$ for the surface reflected intensity, $k = 6$ for the deviated intensity. The slit was inclined to the diffraction plane by a few degrees. (a) shows the slit image without SAW excitation and some contrast due to residual strain at the surface. Topographs (b) to (d) were taken with increasing film distance as indicated. See text.

Figure 6. : Calculated intensity profiles for a slightly inclined slit neglecting orientation contrast effects (short film distance). This distribution has to be compared with Fig. 5(b). Note that the direction of the streaks is not exactly following the acoustic wave fronts.

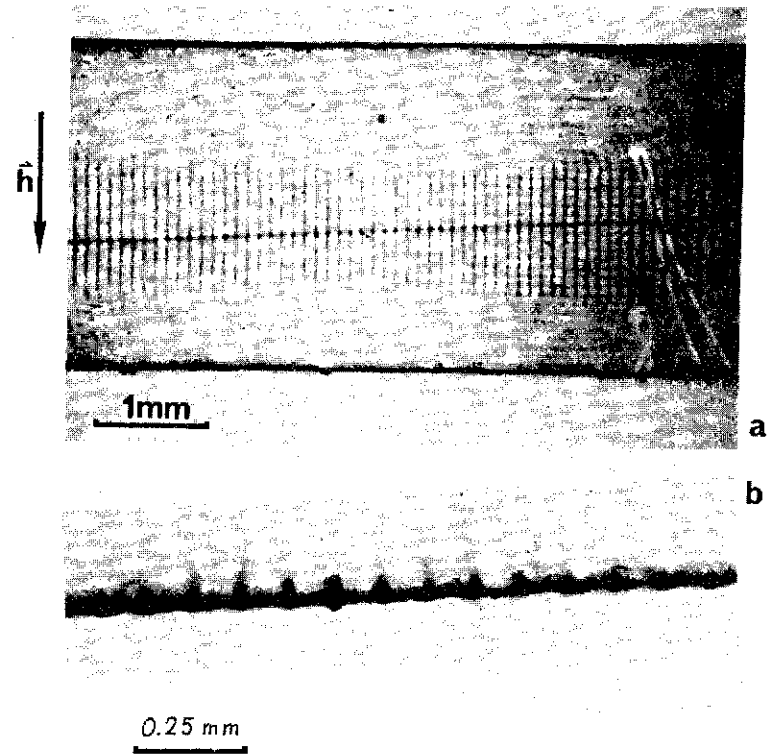


Fig. 5

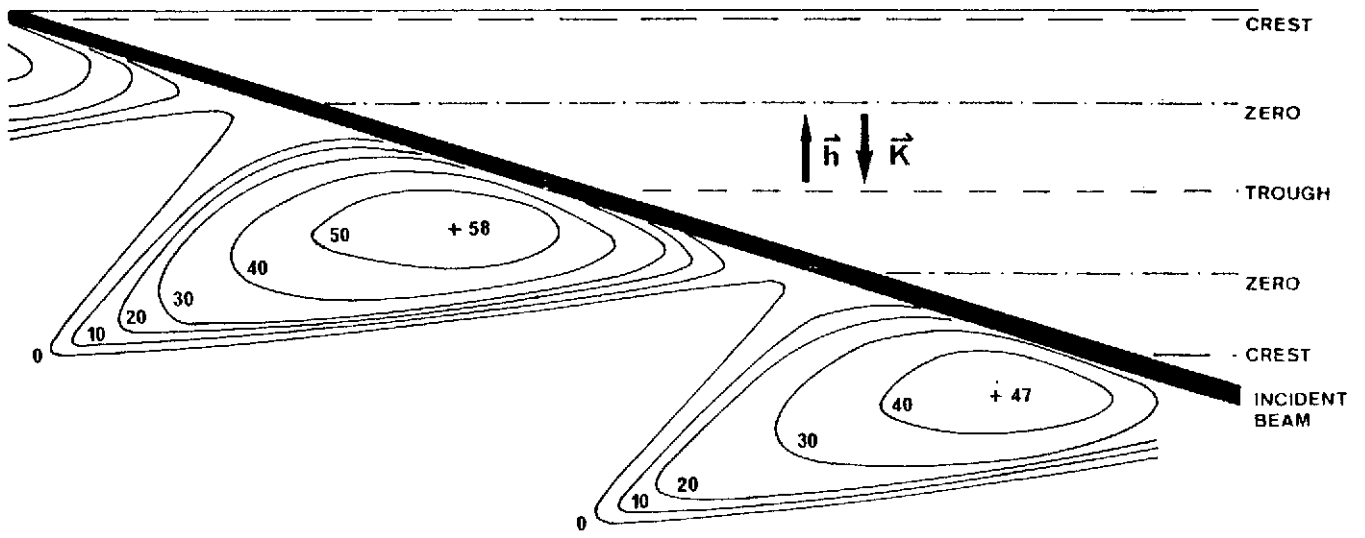


Fig. 3

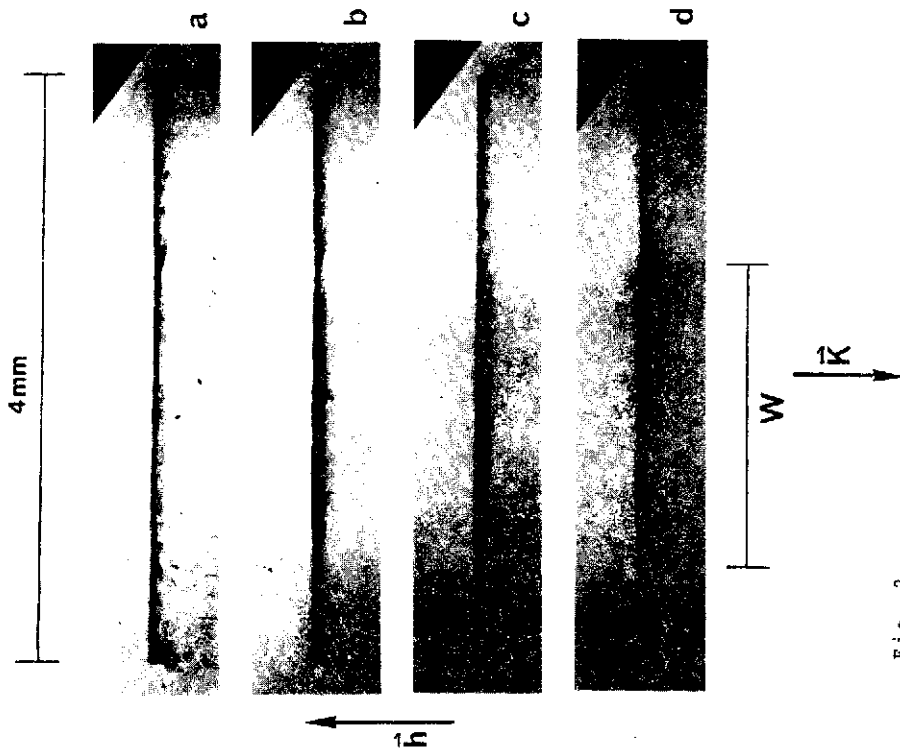


Fig. 2

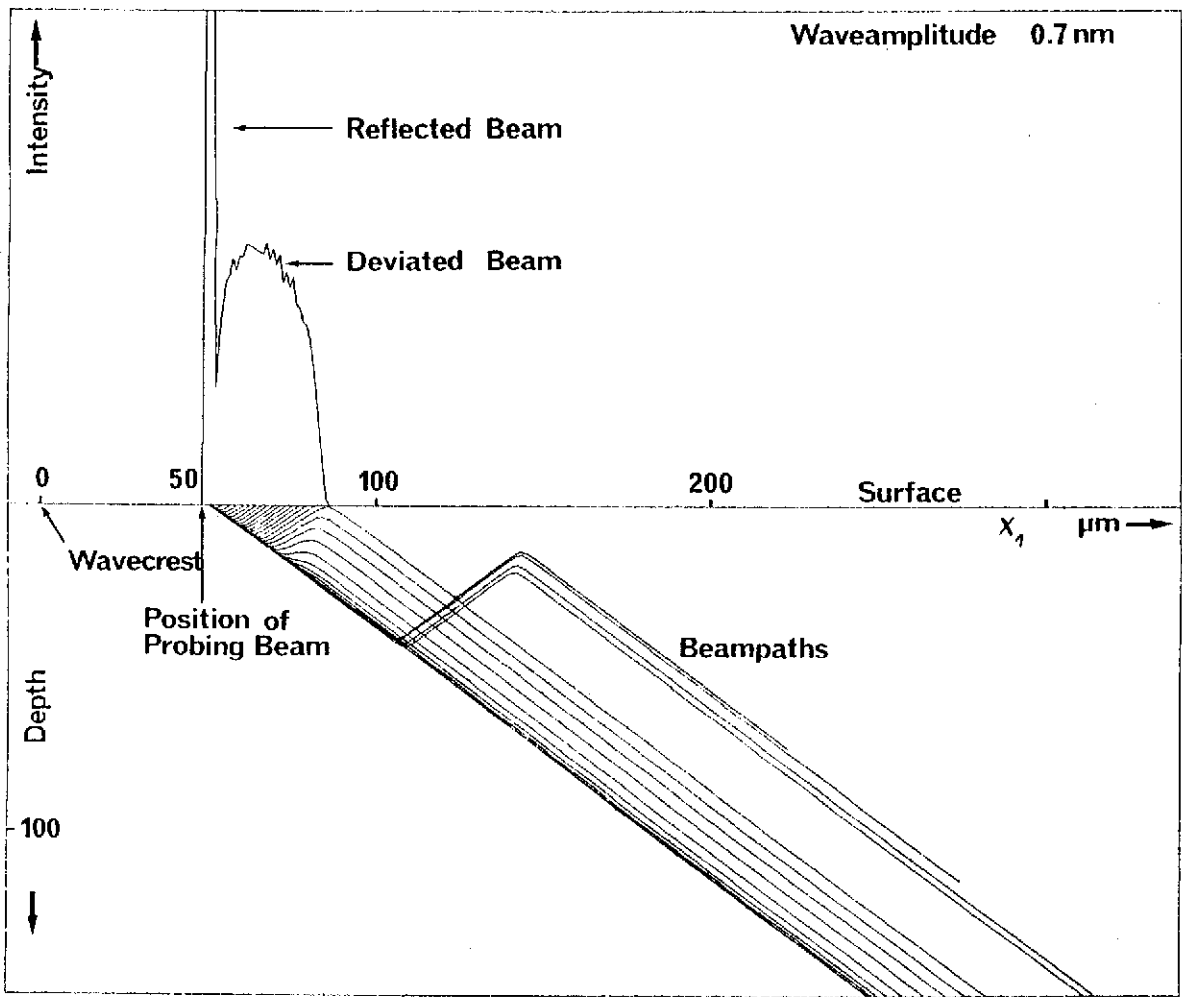


Fig. 4a

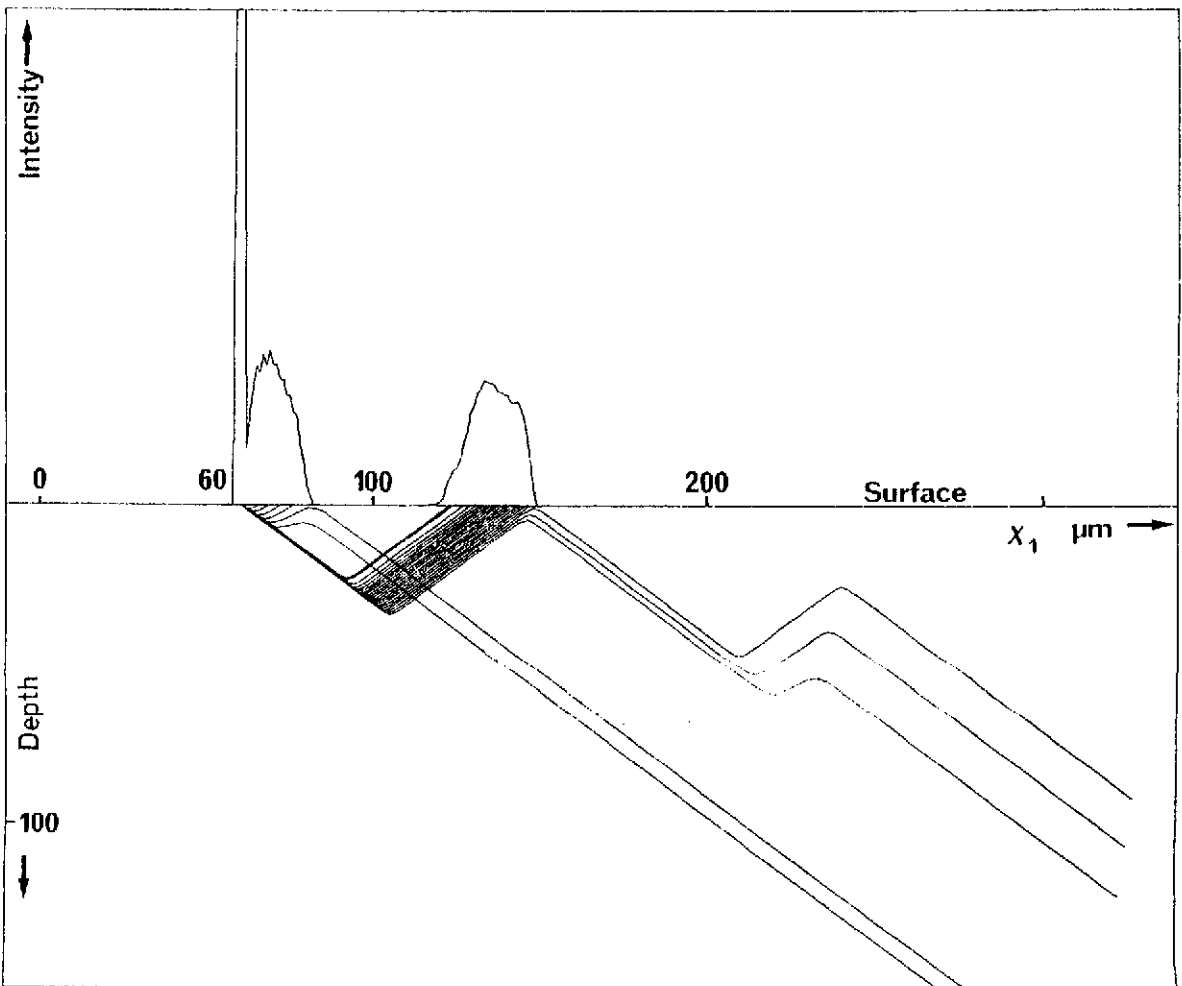


Fig. 4b

0k0 Braggplanes in YZ-LiNbO₃
deformed by a SAW

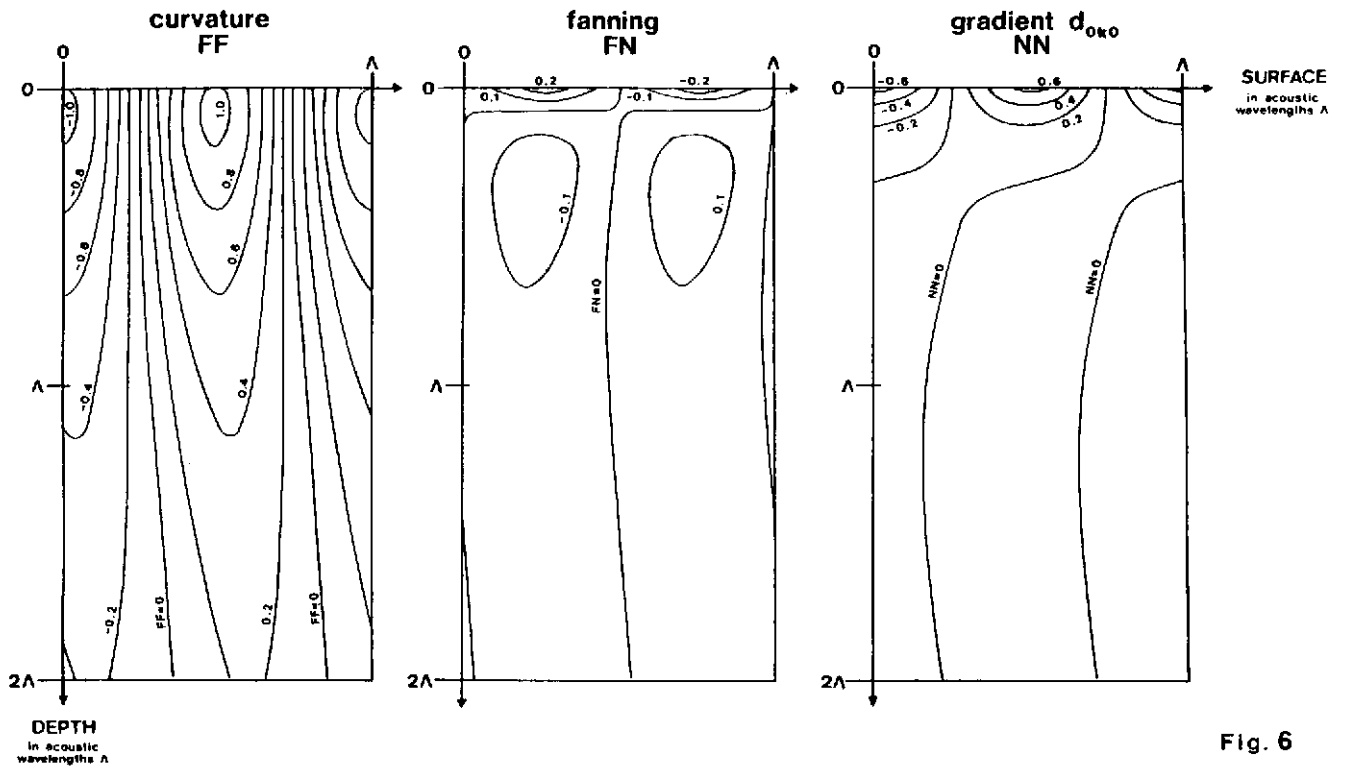


Fig. 6

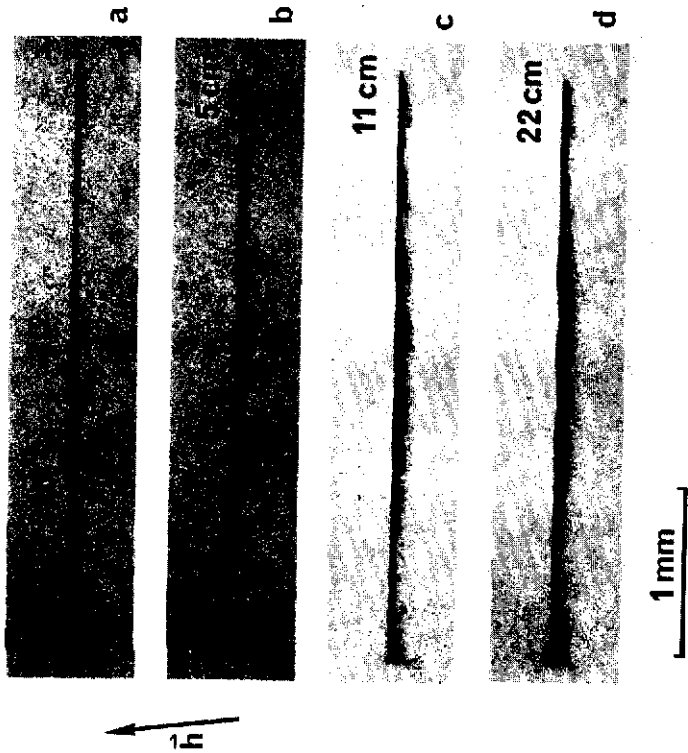


Fig. 5

